



HAL
open science

Quantitative Ultrasound in Ex Vivo Fibrotic Rabbit Livers

Emilie Franceschini, Jean-Michel Escoffre, Anthony Novell, Laurent Auboire, Vanda Mendes, Yanis Bénane, Ayache Bouakaz, Olivier Basset

► **To cite this version:**

Emilie Franceschini, Jean-Michel Escoffre, Anthony Novell, Laurent Auboire, Vanda Mendes, et al.. Quantitative Ultrasound in Ex Vivo Fibrotic Rabbit Livers. *Ultrasound in Medicine & Biology*, 2019, 45 (7), pp.1777-1786. 10.1016/j.ultrasmedbio.2019.02.013 . hal-02200101

HAL Id: hal-02200101

<https://hal.science/hal-02200101>

Submitted on 31 Jul 2019

HAL is a multi-disciplinary open access archive for the deposit and dissemination of scientific research documents, whether they are published or not. The documents may come from teaching and research institutions in France or abroad, or from public or private research centers.

L'archive ouverte pluridisciplinaire **HAL**, est destinée au dépôt et à la diffusion de documents scientifiques de niveau recherche, publiés ou non, émanant des établissements d'enseignement et de recherche français ou étrangers, des laboratoires publics ou privés.

Quantitative ultrasound in *ex vivo* fibrotic rabbit livers

Emilie Franceschini^{a,*}, Jean-Michel Escoffre^b, Anthony Novell^b, Laurent Auboire^b, Vanda Mendes^b, Yanis M. Benane^c, Ayache Bouakaz^b, Olivier Basset^c

^a*Aix-Marseille Université, CNRS, Centrale Marseille, LMA, Marseille, France*

^b*UMR 1253, iBrain, Université de Tours, Inserm, Tours, France*

^c*Univ Lyon, INSA-Lyon, Université Claude Bernard Lyon 1, UJM-Saint Etienne, CNRS, Inserm, CREATIS UMR 5220, U1206, F-69621, Lyon, France*

Abstract

Liver fibrosis is the common result of chronic liver disease. Diagnosis and grading liver fibrosis for patient management is mainly based on blood tests and hepatic puncture-biopsy, which is particularly invasive. Quantitative UltraSound (QUS) techniques provide insight into tissue microstructure and are based on the frequency-based analysis of the signals from biological tissues. This study aims to quantify how spectral-based QUS parameters change with fibrosis grade. The changes in QUS parameters of healthy and fibrotic rabbit liver samples were investigated and were compared to the changes in liver stiffness using shear wave elastography. Overall, the acoustic concentration (EAC) was found to decrease with increasing fibrosis grade while the effective scatterer size (ESD) was found to be higher in fibrotic livers when compared to normal liver. The result of this study indicates that the combination of three QUS parameters (stiffness, ESD and EAC) provides the best classifi-

*Corresponding Author: Dr. Franceschini Emilie, Aix-Marseille Université, CNRS, Centrale Marseille, LMA, Marseille, France ; Email, franceschini@lma.cnrs-mrs.fr; Tel: +33 (0)4 84 52 42 86

cation performance, especially for classifying healthy and fibrotic livers.

Keywords: Quantitative ultrasound, Backscatter coefficient, Stiffness,
Fibrotic liver

1 INTRODUCTION

2 Liver fibrosis results from the chronic damage to the liver tissue in associa-
3 tion with the excessive accumulation of extracellular matrix (ECM) proteins,
4 which is a hallmark feature of a wide variety of chronic liver diseases ([Bataller](#)
5 [& Brenner 2005](#)). In the Western lifestyle countries, the most common causes
6 of hepatic fibrosis are chronic Hepatitis C Virus infection, nonalcoholic steato-
7 hepatitis and alcohol abuse ([Pellicoro et al. 2014](#)). The accumulation of ECM
8 proteins, specifically the collagen, alters the architecture of hepatic tissue by
9 forming fibrous wounds. The subsequent development of nodules of regen-
10 erating hepatocytes outlines the cirrhosis ([Lee et al. 2014](#)). This last one
11 leads to increased intrahepatic resistance to blood flow and hepatocellular
12 dysfunction, which induce a portal hypertension and hepatic insufficiency,
13 respectively.

14 Hepatic puncture-biopsy is the gold standard method to stage liver fi-
15 brosis, a biomarker of advanced liver disease ([Lee et al. 2018](#)). However,
16 liver biopsy is an invasive and potentially painful technique. In addition,
17 the heterogeneity of pathological liver tissue may lead to a selection bias of
18 the biopsy ([Fernandez-Salazar et al. 2011](#)). In this context, several ultra-
19 sound elastography methods (such as transient elastography, acoustic radia-
20 tion force impulse or shear wave elastography (SWE)) have been developed
21 for the noninvasive assessment of liver stiffness, as a Quantitative Ultra-
22 Sound (QUS) imaging biomarker for detection, staging, and monitoring of
23 liver fibrosis ([Tang et al. 2015](#)). Indeed, the collagen deposition and other
24 microstructural changes associated with hepatic fibrosis induce parenchymal
25 rigidity. This liver stiffness increases with higher fibrosis stages. Nowadays,

26 the liver stiffness is used to evaluate the gravity of liver disease, to manage
27 treatment decision and to assess response to treatment (Bhat et al. 2017,
28 Chen et al. 2018, Ippolito et al. 2018). Using current histological techniques
29 with hematoxylin/eosin and picrosirius red staining, pathologists classify the
30 different fibrosis stage using ordinal scores (*i.e.*, from stage 0 to stage 6
31 with Ishak grading) while ultrasound imaging data provide a dichotomized
32 categorization of fibrosis stages including the significant ($\text{stage} \geq 2$) and ad-
33 vanced ($\text{stage} \geq 4$) liver fibrosis stages (Tang, et al. 2015). This different
34 classification observed between histological and imaging techniques might be
35 explained by the sensitivity of both techniques. Indeed, pathologists perform
36 a semi-quantitative analysis of the location and amount of excess collagen but
37 also microstructural changes in the liver tissue architecture (Hui et al. 2004,
38 Kleiner et al. 2005, Theise 2007). Such histological analysis demonstrated
39 that there is no linear correlation between the fibrosis stage and the total
40 amount of collagen, thus suggesting that fibrosis stage is not stated exclu-
41 sively by the total collagen content (Calvaruso et al. 2009, Xu et al. 2014).
42 Indeed, the total amount of collagen remains almost stable from the stage 0
43 to higher stages, until an advanced fibrosis stage is reached, subsequently the
44 total collagen content exponentially increases. These studies clearly reported
45 that the intra-hepatic location of collagen and the liver tissue remodeling
46 contribute to the fibrosis stage. Consequently, the exponential relationship
47 described between the liver stiffness and the fibrosis stage strongly suggests
48 that ultrasound elastography is more a direct biomarker of total amount of
49 collagen than fibrosis stage.

50 To overcome these limitations, combinations of non-invasive QUS tech-

51 niques can be used to improve accuracy and to provide a comprehensive
52 assessment of different stages of liver fibrosis. Spectral-based QUS tech-
53 niques using the parameterization of the backscatter coefficient (BSC) have
54 demonstrated success in many preclinical and clinical applications for tissue
55 characterization (Oelze & Mamou 2016). Specifically, a scattering model is
56 fit to the measured BSC and the fit parameters can provide a meaningful
57 description of the tissue microstructure (*i.e.*, scatterer size, shape, scattering
58 strength and spatial organization). One of the most popular scattering mod-
59 els is the spherical Gaussian model (SGM) developed by Lizzi (Lizzi et al.
60 1986). This model describes tissue as a random medium composed of spher-
61 ical structures having continuous spherical impedance fluctuation following
62 a spherical Gaussian curve, and yields two QUS parameters: the average
63 effective scatterer size (ESD) and the acoustic concentration (EAC) (*i.e.*,
64 the product of the scatterer number density and the square of the relative
65 impedance difference between scatterers and the surrounding medium). Some
66 spectral-based QUS studies have been performed to characterize liver fibro-
67 sis. In clinical trials, the BSCs at the center frequency of 3 MHz were found
68 to be higher in patients with liver cirrhosis, when compared to a healthy
69 patient group (O'Donnell & Reilly 1985, Lu et al. 1999). In *ex vivo* exper-
70 iments, the attenuation coefficient, sound speed and integrated backscatter
71 coefficient with a 20 MHz pulse-echo system allowed a reasonable segregation
72 of patient groups suffering from different fibrosis grades (Meziri et al. 2005).

73 This study aims to quantify how spectral-based QUS parameters change
74 with fibrosis grade. Liver fibrosis was induced by repeated subcutaneous
75 injections of carbon tetrachloride (CCl₄) in the neck of rabbits. Attenuation

76 and backscatter coefficients were estimated over a wide frequency range (up
77 to 40 MHz) from fresh rabbit liver samples using the spectral difference
78 method and the reference phantom method, respectively. The two QUS
79 parameters (ESD and EAC) were estimated by fitting the measured BSC to
80 an estimated BSC calculated with the SGM theoretical model. The changes
81 in QUS parameters of healthy and fibrotic livers were investigated and were
82 compared to the changes in liver stiffness using SWE. Finally, we evaluated
83 whether correctly classifying fibrotic livers was possible based on these QUS
84 estimates.

85 MATERIAL AND METHODS

86 *Rabbit liver fibrosis model*

87 All procedures were performed in accordance with French and Interna-
88 tional ethical guidelines and were approved by the National Committee for
89 Animal Care and Ethics in Animal Experiments (No. 2016020116011353-
90 3872). Eighteen New Zealand white male rabbits (Charles Rivers, Bois des
91 Oncins, France) were housed in a temperature-controlled room (23°C) with
92 12:12-h light-dark cycle in isolation cages. Food and water were presents ad
93 libitum.

94 During the injection protocol and B-mode imaging, the rabbits were anes-
95 thetized by 3% isoflurane (Isoflo, Coveto, Limoges, France) and oxygen via
96 a facial oxygen mask in place throughout the procedure. This anesthesia
97 was limited to 20 min, and a thermostatically controlled pad was used to
98 maintain body temperature at about 37°C plate. The rabbits were 9 weeks
99 old at the beginning of the experiment, weighing in average 2.5 ± 0.2 kg. To

100 induce liver fibrosis, a dose of 0.2 mL/kg CCl₄ (Sigma-Aldrich, St. Louis,
101 MO) as a 50% (v/v) solution in olive oil was subcutaneously administered
102 twice a week during several successive weeks (from 3 up to 12 weeks) because
103 the grade of liver fibrosis is related to the duration of CCl₄ injection (Li et
104 al. 2018). Experimentation used 18 animals divided in 5 groups. The first 4
105 groups corresponded to injection protocols of 3 weeks ($n=4$ rabbits), 6 weeks
106 ($n=4$ rabbits), 9 weeks ($n=3$ rabbits) and 12 weeks ($n=3$ rabbits), and the
107 fifth group ($n=4$ rabbits) were left untreated to generate control data. The
108 progression of liver fibrosis was monitored twice a week using an Acuson Se-
109 quoia ultrasound system (Siemens Healthcare GmbH, Erlangen, Germany)
110 with an Acuson 15L8 ultrasound probe. An expert medical doctor (L.A.)
111 reviewed the ultrasound B-scans of healthy and fibrotic livers.

112 After liver fibrosis induction, the rabbits were euthanized under anesthe-
113 sia by i.v. injection of 1 mL/kg Doléthal (Vétoquinol S.A., Magny-Vernois,
114 France). For each rabbit, the liver was excised and immersed in degassed
115 saline solution to be ultrasonically imaged for QUS analysis as described be-
116 low. (*Ex vivo* study was conducted to allow high frequency measurements
117 up to 40 MHz and to explore liver microstructure properties, as discussed
118 later in the section "Results and Discussion".)

119 *Shear wave elastography (SWE)*

120 Real-time SWE was performed using an Aixplorer UltraFastTM system
121 (SuperSonic Imagine, Aix-en-Provence, France), equipped with a linear array
122 probe (SL15-4) with a center frequency of 8.5 MHz in order to determine the
123 liver stiffness *ex vivo*. Elasticity estimates were color-coded creating a 2D
124 quantitative SWE image of liver stiffness, which was shown in box form over

125 a conventional B-mode image. For each animal, liver stiffness measurements
126 were acquired on all three liver lobes. For each lobe, three round regions of
127 interest (ROIs) were placed in the box on the gray-scale ultrasound image.
128 Liver stiffness was expressed as the mean \pm standard deviation of elastic
129 modulus (kPa) of three liver lobes.

130 *Spectral-based quantitative ultrasound method*

131 High-frequency ultrasound imaging was performed using the Vevo 2100
132 imaging system (FUJIFILM - VisualSonics Inc, Toronto, Canada). Two lin-
133 ear array probes, MS250 of center frequency 20 MHz and MS550 of center
134 frequency 40 MHz, were used in B-mode in order to estimate tissue mi-
135 crostructures on the three liver lobes of each rabbit. For each liver lobe, ten
136 consecutive frames were acquired on three different locations. One frame is
137 formed from 512 scan lines. The orientation and the position of the probe
138 were chosen to prevent the presence of specular echoes originating from the
139 veins or arteries in the scan plane.

140 For the two linear array probes, reference scans were acquired from a
141 well-characterized reference phantom after conducting the experiments on
142 rabbit livers with the same imaging system settings (Yao et al. 1990). The
143 reference phantom was provided by the University of Wisconsin (WI, USA)
144 and consisted of 6g/L of glass beads with radii ranging from 0.4 to 6 μm in
145 a gel-surrounding medium. The reference phantom has been characterized
146 to measure its backscatter coefficient BSC_{ref} on the 10-40 MHz frequency
147 bandwidth using a planar reflector and focused transducers having different
148 center frequencies 10, 20 and 35 MHz (Chen et al. 1997). The measured
149 BSC_{ref} magnitude was comparable with backscatter coefficient magnitudes

150 from rabbit liver tissues (for example, $BSC_{\text{ref}}=0.0018 \text{ cm}^{-1}.\text{sr}^{-1}$ at 10 MHz
 151 and $BSC_{\text{ref}}=0.0166 \text{ cm}^{-1}.\text{sr}^{-1}$ at 20 MHz). The sound speed and acoustic
 152 attenuation were quantified by the manufacturer using a standard narrow-
 153 band through-transmission substitution technique (Madsen et al. 1982). The
 154 sound speed was equal to 1535 m/s and the measured attenuation was fitted
 155 with the following function: $\alpha_{\text{ref}}=0.055 f^{1.544} \text{ dB/cm}$, where f is the frequency
 156 in MHz. This fitting curve is valid in the frequency range from 10 to 40 MHz.

Signal analysis for attenuation and BSC computation is performed in selected ROIs placed on the ultrasound B-mode images of liver lobe. The ROIs are drawn as large as possible with at least 200 scan lines. QUS images based on BSC analysis depict tissue properties in a system-independent manner. The reference phantom technique was employed for local attenuation and BSC estimation to account for the electromechanical system response and the depth-dependent diffraction and focusing effects of the ultrasound beam (Labyed & Bigelow 2011, Yao et al. 1990). The local attenuation α_s was first estimated using the spectral log difference method with the 40-MHz probe (Labyed & Bigelow 2011). The measured BSC_{meas} was then computed using the reference phantom technique with both 20-MHz and 40-MHz probes (Yao et al. 1990). The BSC_{meas} of the liver sample was computed as follows:

$$BSC_{\text{meas}}(f) = BSC_{\text{ref}}(f) \frac{\overline{P_{\text{meas}}}(f)}{\overline{P_{\text{ref}}}(f)} e^{4z(\alpha_s(f) - \alpha_{\text{ref}}(f))} \quad (1)$$

157 where f is the frequency, BSC_{ref} is the BSC of the reference phantom measured by using a planar reflector and focused transducers (as described previously); $\overline{P_{\text{meas}}}$ and $\overline{P_{\text{ref}}}$ are the power spectra for the liver sample and reference
 158 phantom at equivalent depth z . The last term (*i.e.*, the exponential function)
 159 compensates for attenuation effects. This procedure yielded a BSC_{meas} for
 160
 161

162 each probe: in the 10-30 MHz bandwidth with the MS250 probe and in the
 163 20-40 MHz bandwidth with the MS550 probe. The resultant two BSC_{meas}
 164 could be combined to yield a single BSC_{meas} over the combined bandwidth of
 165 the two transducers (*i.e.*, 10 - 40 MHz). More specifically, there is at least one
 166 intersection point (at frequency f_I) between the two BSC_{meas} curves within
 167 the 20-30 MHz frequency bandwidth, such that the two BSC_{meas} curves are
 168 combined by using the BSC_{meas} measured with the MS250 probe in the [10
 169 MHz - f_I] bandwidth and the BSC_{meas} measured with the MS550 probe in
 170 the [f_I -40 MHz] bandwidth.

For each ROI, two QUS parameters, namely the ESD and EAC, were obtained by fitting the measured BSC_{meas} with the spherical Gaussian model (Insana et al. 1990). The spherical Gaussian model is based on several approximations (Born, far-field, incident plane wave, isotropic medium) for soft tissue scattering. Based on these approximations, the BSC is modeled using a spatial autocorrelation function describing the size, shape, acoustic properties and distribution of the scatterers in the medium; and is expressed as follows (Insana et al. 1990):

$$BSC_{\text{SGM}}(k) = \frac{k^4 V_s^2 n_z}{4\pi^2} e^{-2k^2 d^2} = \frac{k^4 V_s^2 n_z}{4\pi^2} e^{-0.827k^2 a^2}, \quad (2)$$

171 where k is the wavenumber, n_z is the acoustic concentration (*i.e.*, $EAC=n_z$),
 172 d is the correlation distance that characterized the continuous isotropic medium
 173 and $V_s = (2\pi d^2)^{3/2}$. The effective scatterer radius a is related to the corre-
 174 lation distance d by setting values of V_s for a continuum model equal to the
 175 volume of an effective sphere of radius a : $V_s = (2\pi d^2)^{3/2} = (4/3)\pi a^3$ (Insana
 176 et al. 1990). The ESD has been related to the size of dominant scatterers
 177 in liver tissues (*i.e.*, $ESD=2a$). The reported ESD and EAC parameters are

178 averaged over the three measurements performed on each lobe.

179 *Histopathology*

180 Livers were fixed in the 4% formol solution (Labo-moderne, Paris, France).
181 Then, histological samples were embedded in paraffin, cut at approximately
182 5 μm , and prepared using conventional hematoxylin/eosin and picrosirius
183 red protocols (Novaxia, Saint-Laurent Nouan, France). These tissue sections
184 were examined by light microscopy on a Leica Diaplan microscope. Histolog-
185 ical slides were reviewed by an expert hepatopathologist (Le Net Pathologist
186 Consulting, Amboise, France). The liver fibrosis was graded according to the
187 Ishak grading ([Ishak et al. 1995](#)), a grading with a 7-tier scale offering high
188 discriminant descriptive power suitable for research purposes ([Almpanis et
189 al. 2016](#)).

190 **RESULTS AND DISCUSSION**

191 *Effects of CCl₄ on rabbit behavior and on liver anatomy*

192 Upon visual inspection of the rabbits, all CCl₄ treated animals were gen-
193 erally less groomed and less active compared to untreated control group. In
194 addition, 3 CCl₄ treated animals were dead before the study ended and a
195 significant loss of body weight (*i.e.*, > 10% of initial body weight) was also
196 observed in 7 out of 15 surviving animals in the first three weeks of CCl₄
197 injection (Table 1).

198 In the present study, B-mode ultrasound imaging was chosen to monitor
199 the effects of CCl₄ administration on liver anatomy. During the two first
200 weeks of CCl₄ injection, neither liver failure nor behavioral anomalies (*i.e.*,

201 loss of appetite, dehydration, loss of body weight, breathing difficulties) was
202 observed in all studied rabbits. However, after 3 weeks of CCl₄ injection,
203 abdominal ultrasound imaging revealed an increase in the liver echogenicity
204 in all CCl₄ treated animals. Figures 1(a) and 1(b) show representative B-
205 mode images of healthy and fibrotic (grade 5) liver with 12-weeks of CCl₄
206 injection. The fibrotic liver shown in Fig. 1(b) presents an accumulation
207 of fluids in the abdominal cavity, also called ascites, that suggests a hepatic
208 failure. The qualitative analysis of abdominal images from all the studied
209 rabbits should suggest that the amount of fluid in the abdominal cavity
210 increased with the number of CCl₄ injections. At the study end, the necropsy
211 confirmed the presence of ascites in the abdominal cavity of all CCl₄ injected
212 animals. In addition, these rabbits had a strong discoloration of the liver
213 tissues in comparison with the control group, as it can be observed in Figs.
214 1(c) and 1(d).

215 *Histopathological analysis*

216 To confirm the induction of liver fibrosis, histopathological analyzis was
217 performed on liver tissues. As shown in Figure 2, the picosirius red stain-
218 ing clearly indicates an excessive accumulation of collagen around the lobule
219 structures confirming that the repetitive administrations of CCl₄ induced
220 liver fibrosis. Despite intra- and inter-individual variations in the liver re-
221 sponse to CCl₄ administration were observed, the amount of fibrosis was
222 homogeneous among three liver lobes for each rabbit. In addition, minimal
223 haemosiderosis (*i.e.*, indicator of previous hemorrhage) was present in all
224 treated animals. Table 2 gives the relationship between the fibrosis grades
225 and the weeks of CCl₄ injection. The amount of fibrosis increases with the

226 duration of CCl4 injection protocol, as expected. Based on Ishak grading,
227 the rabbit livers were classified within different grades (denoted G in the fol-
228 lowing): G0 with no fibrosis (4 rabbits), G1 (2 rabbits), G2 (2 rabbits), G3
229 (2 rabbits), G4 (3 rabbits) and G5 (2 rabbits). No liver cirrhosis (G6) was
230 detected.

231 *QUS parameter estimates*

232 Typical examples of shear wave elastography images are shown in Fig. 3,
233 and the average Young's modulus of all grades are summarized in Table 3.
234 Young's modulus values were on the order of several thousands of Pascals
235 and noticeably increased with the fibrosis grade, as expected. The statistical
236 analysis using the Pearson correlation method reveals that the liver fibrosis
237 score was positively correlated with the Young's modulus ($p < 0.0001$), as
238 expected.

239 The attenuation was found to depend linearly on frequency, within the
240 20-40 MHz frequency bandwidth. The mean values and standard deviation
241 of attenuation coefficients were equal to 0.58 ± 0.13 , 0.85 ± 0.07 , 0.87 ± 0.09 ,
242 0.83 ± 0.08 , 0.89 ± 0.07 and 0.91 ± 0.09 dB/cm/MHz for G0 (normal), G1, G2,
243 G3, G4 and G5, respectively. Averaged attenuation coefficient was thus
244 found to be higher in fibrotic livers. This trend correlates well with pre-
245 vious experimental results conducted at 20 MHz by (Meziri et al. 2005):
246 attenuation coefficients were found to be equal to 0.76 dB/cm/MHz and 1.06
247 dB/cm/MHz for normal and cirrhotic livers, respectively.

248 Typical examples of measured BSC_{meas} are shown in Fig. 4. The BSC_{meas}
249 magnitudes from fibrotic livers were greater than those from normal liver in
250 the 10-22 MHz frequency bandwidth, as observed previously in the literature

251 (O'Donnell & Reilly 1985, Lu et al. 1999). Table 3 also displays the average
252 and standard deviations of the spectral-QUS estimates for the fibrotic grade
253 livers. Overall, the EAC decreased with increasing fibrosis grade and the
254 ESD was found to be higher in fibrotic livers when compared to normal liver
255 for both 10-20 MHz and 10-40 MHz frequency bandwidths.

256 The abilities of QUS parameters to differentiate among grades of fibrosis
257 were assessed using 1-way ANOVA. Statistically significant differences were
258 quantified using p values < 0.05 . The p values are shown in Table 3. For
259 example, p -values for G0 versus (vs) G1 refers to the significance of QUS pa-
260 rameters estimated from animals with no fibrosis with G0 and fibrosis with
261 G1; and p -values for [G1-2] vs [G3-5] refers to the significance of QUS parame-
262 ters estimated from animals with moderate fibrosis with G1 and G2 (denoted
263 G1-2) and with severe fibrosis \geq G3 (denoted G3-5). The Young's modulus,
264 ESD and EAC parameters (p value < 0.05) can be used to differentiate be-
265 tween G0 and G1, and to differentiate between normal and fibrotic livers.
266 The Young's modulus and EAC parameters (p value < 0.05) can be used to
267 differentiate between moderate (G1-2) and severe (G3-5) fibrosis (but not
268 the ESD). None of the parameters enables the graduation of the fibrosis in 6
269 grades (from G0 to G5). Only the ESD and EAC parameters estimated at
270 high frequencies using the 10-40 MHz could differentiate G2 and G3.

271 *Usefulness of high frequency measurements*

272 To our knowledge, it is the first time that high frequency measurements
273 up to 40-MHz center frequency probe are reported in *ex vivo* livers. High fre-
274 quency measurements cannot be used in real clinical condition, but are useful
275 to obtain a more robust estimation of the scatterer size and to progress fur-

276 ther in the understanding of backscattering from fibrotic livers. It is very
277 interesting to observe the frequency-dependent of the BSC_{meas} in the case of
278 normal liver that shows a peak of magnitude around 30 MHz (see black curve
279 in Fig. 4). The ESD estimated with the SGM was found to be equal to 19.5
280 μm in the 10-40 MHz frequency bandwidth. However, it is known that the
281 SGM may not bring a meaningful description of the tissue microstructure in
282 the case of complex media, such as dense and/or polydisperse scattering me-
283 dia (Franceschini et al. 2016). In order to better interpret this peak around
284 30 MHz, the BSC_{meas} was fitted with the polydisperse structure factor model,
285 allowing the simultaneous estimation of the scatterer diameter distribution,
286 the volume fraction and the relative impedance contrast (Franceschini et al.
287 2016). As shown in Fig. 4, the polydisperse structure factor model suggests
288 that this peak is representative of $ESD \approx 28 \mu\text{m}$, which is quite close from the
289 hepatocyte diameter $d \approx 26 \mu\text{m}$ (as deduced from the area surface of hepa-
290 tocytes observed in histological slices). However, even with high frequency
291 measurements and advanced scattering models (such as the structure factor
292 model), we were not able to establish a relationship between QUS scatterer
293 property estimates and actual fibrotic liver structures. *Note that the QUS*
294 *parameters obtained from the structure factor model with fibrotic livers were*
295 *not shown in the present study because the SGM was found to be more effi-*
296 *cient than the structure factor model for grading the fibrotic liver (data not*
297 *shown).*

298 Figure 5 shows typical examples of B-mode images obtained from *ex vivo*
299 healthy and fibrotic livers using the 40-MHz center frequency probe. The B-
300 mode images of healthy liver display hyper-echogenic structures with hexag-

301 onal shapes corresponding to liver lobule structures, whereas fibrotic livers
302 show more homogeneous speckle. So the connective tissue of lobular bound-
303 aries plays also an important contribution in the scattering process, in addi-
304 tion to the contribution of the cellular/hepatocyte scattering. Future studies
305 should be focused on the understanding of scattering contribution from con-
306 nective tissue of lobular boundaries, collagen fibers and cellular/hepatocyte
307 microstructure in normal and fibrotic livers, using for example acoustic mod-
308 els of tissue microstructure, termed impedance maps (Mamou et al. 2005,
309 Luchies & Oelze 2005, Tamura et al. 2017)

310 *Fibrosis classification based on QUS estimates*

311 The ability of Young's modulus and spectral-QUS parameters for clas-
312 sifying liver grades was studied using the Gaussian Mixture Model (GMM)
313 (McLachlan & Peel 2000). For this study, we use only the ESD and EAC
314 estimated within the 10-20 MHz bandwidth, which corresponds to a more
315 accessible frequency bandwidth in usual ultrasound devices. The classifica-
316 tion was performed by fitting a Gaussian mixture distribution model to the
317 N classes of the QUS data. The classification was tested for three classes
318 ($N=3$): no fibrosis with G0 (4 animals), moderate fibrosis with G1 and G2 (4
319 animals) and severe fibrosis with G3, G4 and G5 (7 animals). When consider-
320 ing the stiffness parameter or the tissue microstructure parameters (ESD and
321 EAC), the classification was first performed by using all the 135 data (corre-
322 sponding to 15 animals \times 3 lobes/animal \times 3 measurements/lobe). The data
323 were separated in two groups: half of the 135 data were assigned randomly to
324 a training group, and the other half was assigned to a validation group to test
325 the classification on the model obtained with the training group. Figures (6a-

326 b) represent the confusion matrices that summarize the classification results
327 when considering the Young's modulus alone and the spectral-QUS param-
328 eters alone. When combining the three QUS parameters (Young's modulus,
329 ESD and EAC), the classification was performed by using the QUS param-
330 eters averaged over the three measurements for each studied lobe (*i.e.*, 45
331 measurements corresponding to 15 animals \times 3 lobes/animals), because the
332 stiffness and tissue microstructure measurements were not performed on the
333 same ROI. In that case, the separation in training and validation groups was
334 not performed because of the low number of data but a classification using
335 the leave-one-out cross-validation was used. For comparison purpose, the
336 GMM associated with the leave-one-out cross-validation was used by pro-
337 cessing the same 45 averaged measurements when considering the stiffness
338 parameter alone and the spectral-QUS parameters alone. The confusion ma-
339 trices obtained from leave-one-out cross-validation are given in Figs. (6c-e),
340 when using the Young's modulus alone, the spectral-QUS parameters alone,
341 and the combination of spectral-QUS parameters with Young's modulus, re-
342 spectively.

343 Overall, the separation in training and validation groups allows us to bet-
344 ter classifying the lobes when compared to the leave-one-out cross-validation
345 (see Figs. 6a-d). It can be observed that the class G0 is always better
346 classified ($P_c \geq 83\%$ of correctly classified lobes) when the spectral-QUS pa-
347 rameters (ESD and EAC) are considered, whatever the classification methods
348 used (see Fig. 6b for the separation in training and validation groups, and
349 see Figs. 6(d-e) for the leave-one-out cross-validation). The fibrotic livers
350 (classes G1-2 and G3-5) are also better classified using the combination of

351 the three QUS parameters (Young’s modulus, ESD and EAC), when com-
352 pared to the classifications obtained with the spectral-QUS parameters or
353 with the Young’s modulus alone (Figs. 6(c-e)).

354 The results obtained in the present study suggest that the combination of
355 spectral-QUS parameters with Young’s modulus resulted in improved clas-
356 sification compared to Young’s modulus alone. Further study should be
357 conducted on *in vivo* livers to confirm the added value of the spectra-QUS
358 parameters for fibrosis classification. Indeed, the present study is limited to
359 *ex vivo* liver samples, such that the BSC data were simply compensated for
360 liver attenuation. Challenges for *in vivo* application are to correctly account
361 for attenuation effects and transmission losses. Even if previous studies have
362 demonstrated the ability to accurately estimate the BSC and attenuation
363 using the reference phantoms on clinical systems (Wirtzfeld et al. 2010, Han
364 et al. 2017), the QUS parameter variance from *in vivo* application may be
365 higher when compared to those obtained in the present *ex vivo* study and
366 this could affect the classification efficiency.

367 **Conclusion**

368 In summary, the EAC was found to decrease with increasing fibrosis grade
369 and the ESD was found to be higher in fibrotic livers when compared to nor-
370 mal liver. The EAC parameter was shown to be more sensitive to changes
371 in fibrotic tissues when compared to ESD parameter, especially for differ-
372 entiating between moderate (G1-2) and severe (G3-5) fibrosis. The results
373 reported here also suggest that ESD and EAC bring complementary infor-
374 mation to standard stiffness measurements for fibrosis classification, since

375 the combination of the three QUS parameters (Young's modulus, ESD and
376 EAC) provides the best classification performance. Further study should be
377 performed to demonstrate the superiority of the QUS approach combining
378 tissue microstructure and stiffness in human clinical study for classifying liver
379 fibrosis.

380 **Acknowledgements**

381 The authors acknowledge Mrs V. Schubnel (PST Animalerie, Universit de
382 Tours, France) for the animal experience. We are grateful for the technical
383 support from Visualsonics. This work was supported by the French National
384 Research Agency under grant ANR TecSan 11-008-01 (OB), and ANR-11-
385 IDEX-0001-02 (EF) and Inserm grant (JME, AB).

386 Almpanis Z, Demonakou M, Tiniakos D. Evaluation of liver fibrosis:
387 "Something old, something new...". *Annals of gastroenterology* 2016;
388 29:445-53

389 Bataller R, Brenner DA. Liver fibrosis. *J. Clin. Invest.* 2005; 115:1100-00

390 Bhat M, Tazari M, Sebastiani G. Performance of transient elastogra-
391 phy and serum fibrosis biomarkers for non-invasive evaluation of recur-
392 rent fibrosis after liver transplantation: A meta-analysis. *PLoS One* 2017;
393 12:e0185192

394 Calvaruso V, Burroughs AK, Standish R, Manousou P, Grillo F, Leandro
395 G, Maimone S, Pleguezuelo M, Xirouchakis I, Guerrini GP, Patch D, Yu
396 D, O'Beirne J, Dhillon AP. Computer-assisted image analysis of liver col-
397 lagen: relationship to Ishak scoring and hepatic venous pressure gradient.
398 *Hepatology* 2009; 49:1236-44

399 Chen SH, Lai HC, Chiang IP, Su WP, Lin CH, Kao JT, Chuang PH,
400 Hsu WF, Wang HW, Chen HY, Huang GT, Peng CY. Changes in liver
401 stiffness measurement using acoustic radiation force impulse elastography
402 after antiviral therapy in patients with chronic hepatitis C. *PLoS One* 2018;
403 13:e0190455

404 Chen X, Phillips D, Schwarz KQ, Mottley JG, Parker KJ. The measure-
405 ment of backscatter coefficient from a broadband pulse-echo system: a new
406 formulation. *IEEE Trans Ultrason Ferroelectr Freq Control* 1997; 44:515-25

407 Fernandez-Salazar L, Velayos B, Aller R, Lozano F, Garrote JA, Gon-
408 zalez JM. Percutaneous liver biopsy: patients' point of view. *Scand. J.*
409 *Gastroenterol.* 2011; 46:727-31.

410 Franceschini E, de Monchy R, Mamou J. Quantitative characterization of

411 tissue microstructure in concentrated cell pellet biophantoms based on the
412 structure factor model. *IEEE Trans Ultras Ferroelectr Freq Control* 2016;
413 63:1321-1334.

414 Han A, Andre MP, Erdman JW, Loomba R, Sirlin CB, O'Brien WD. Re-
415 peatability and reproducibility of a clinically based QUS phantom study
416 and methodologies. *IEEE Trans Ultras Ferroelectr Freq Control* 2017;
417 64:218-231

418 Hui AY, Liew CT, Go MY, Chim AM, Chan HL, Leung NW, Sung JJ.
419 Quantitative assessment of fibrosis in liver biopsies from patients with
420 chronic hepatitis B. *Liver Int* 2004; 24:611-8

421 Insana MF, Wagner RF, Brown DG, Hall TJ. Describing small-scale struc-
422 ture in random media using pulse-echo ultrasound. *The Journal of the*
423 *Acoustical Society of America* 1990; 87:179-92

424 Ippolito D, Schiavone V, Talei Franzesi CR, Casiraghi AS, Drago SG,
425 Riva L, Sironi S. Real-time elastography: Noninvasive diagnostic tool in
426 the evaluation of liver stiffness in patients with chronic viral hepatitis, cor-
427 relation with histological examination. *Dig Dis* 2018:1-9

428 Ishak K, Baptista A, Bianchi L, Callea F, De Groote J, Gudat F, Denk
429 H, Desmet V, Korb G, MacSween RN, Philips J, Portmann BG, Poulsen
430 H, Scheuer PJ, Schmid M, Thaler H. Histological grading and staging of
431 chronic hepatitis. *Journal of hepatology* 1995; 22:696-9

432 Kleiner DE, Brunt EM, Van Natta M, Behling C, Contos MJ, Cummings
433 OW, Ferrell LD, Liu YC, Torbenson MS, Unalp-Arida A, Yeh M, Mc-
434 Cullough AJ, Sanyal AJ, Nonalcoholic Steatohepatitis Clinical Research
435 N. Design and validation of a histological scoring system for nonalcoholic

436 fatty liver disease. *Hepatology* 2005; 41:1313-21

437 Labyed Y, Bigelow TA. A theoretical comparison of attenuation measure-
438 ment techniques from backscattered ultrasound echoes. *J Acoust Soc Am*
439 2011; 129:2316-24

440 Lee S-J, Kim K-H, Park K-K. Mechanisms of fibrogenesis in liver cirrho-
441 sis: The molecular aspects of epithelial-mesenchymal transition. *World J*
442 *Hepatol* 2014; 6:207-16

443 Li RK, Ren XP, Yan FH, Qiang JW, Lin HM, Tao W, Zhao HF, Chen
444 WB. Liver fibrosis detection and staging: a comparative study of T1rho
445 MR imaging and 2D real-time shear-wave elastography. *Abdominal radi-*
446 *ology* 2018; 43:1713-1722

447 Lizzi FL, Ostromogilsky M, Feleppa EJ, Rorke MC, Yaremko MM. Rela-
448 tionship of ultrasonic spectral parameters to features of tissue microstruc-
449 ture. *IEEE Trans Ultrason Ferroelect Freq Contr.* 1986; 33:319-329

450 Lu ZF, Zagzebski JA, Lee FT. Ultrasound backscatter and attenuation in
451 human liver with diffuse disease. *Ultrasound Med. Biol.* 1999; 25:1047-1054

452 Luchies A, Oelze ML, Using two-dimensional impedance maps to study
453 weak scattering in sparse random media, *J Acoust Soc Am* 2016; 139:1557-
454 1564.

455 McLachlan G, Peel D. *Finite Mixture Models*. Hoboken, NJ: John Wiley
456 & Sons, Inc., 2000.

457 Madsen EL, Zagzebski JA, Insana MF, Burke TM, Frank G. Ultrasonically
458 tissue-mimicking liver including the frequency dependence of backscatter.
459 *Med Phys* 1982; 9:703-10

460 Mamou J, Oelze ML, O'Brien WD, Zachary JF. Identifying ultrasonic

461 scattering sites from three-dimensional impedance maps. *J. Acoust. Soc.*
462 *Am.* 2005; 117: 413-423.

463 Meziri M, Pereira WCA, Abdelwahab A, Degott C, Laugier P. In vitro
464 chronic hepatic disease characterization with a multiparametric ultrasonic
465 approach, *Ultrasonics* 2005; 43:305-313

466 Oelze M, Mamou J. Review of quantitative ultrasound: envelope statistics
467 and backscatter coefficient imaging and contributions to diagnostic ultra-
468 sound, *IEEE Trans Ultrason Ferroelect Freq Contr.* 2016; 63:336-351

469 O'Donnell M, Reilly HF. Clinical evaluation of the B scan. *IEEE Trans.*
470 *Sonics and Ultrasonics* 1985; SU-32:450-457

471 Pellicoro A, Ramachandran P, Iredale JP, Fallowfield JA. Liver fibrosis
472 and repair: immune regulation of wound healing in a solid organ. *Nat.*
473 *Rev. Immunol.* 2014; 14:181-94

474 Tang A, Cloutier G, Szeverenyi NM, Sirlin CB. Ultrasound Elastography
475 and MR Elastography for Assessing Liver Fibrosis: Part 1, Principles and
476 Techniques. *AJR Am J Roentgenol* 2015; 205:22-32

477 Tang A, Cloutier G, Szeverenyi NM, Sirlin CB. Ultrasound Elastogra-
478 phy and MR Elastography for Assessing Liver Fibrosis: Part 2, Diagnostic
479 Performance, Confounders, and Future Directions. *AJR Am J Roentgenol*
480 2015; 205:33-40

481 Tamura K, Franceschini E, Mamou J, Yamaguchi T. Structure factor
482 model-based approach for analyzing two-dimensional impedance map and
483 studying scattering from polydisperse dense media, *IEEE International Ul-*
484 *trasonics Symposium* 2017, 10.1109/ULTSYM.2017.8092125

485 Theise ND. Liver biopsy assessment in chronic viral hepatitis: a personal,

486 practical approach. *Mod Pathol* 2007; 20 Suppl 1:S3-14
487 Wirtzfeld LA, Cross-imaging platform comparison of ultrasonic backscat-
488 ter coefficient measurements of live rat tumors. *J Ultrasound Med* 2010;
489 29:11171123.
490 Xu S, Wang Y, Tai DCS, Wang S, Cheng CL, Peng Q, Yan J, Chen Y,
491 Sun J, Liang X, Zhu Y, Rajapakse JC, Welsch RE, So PTC, Wee A, Hou
492 J, Yu H. qFibrosis: a fully-quantitative innovative method incorporating
493 histological features to facilitate accurate fibrosis scoring in animal model
494 and chronic hepatitis B patients. *Journal of hepatology* 2014; 61:260-69
495 Yao LX, Zagzebski JA, Madsen EL. Backscatter coefficient measurements
496 using a reference phantom to extract depth-dependent instrumentation
497 factors. *Ultrasonic imaging* 1990; 12:58-70.

498 **Tables**

499 **Table 1:** Effect of CCl₄ on survival and loss of body weight.

Weeks of CCl ₄ injection	Loss of body weight (>10% initial)		
	≤3 weeks of CCl ₄	Study end	Survival
0	0/4	0/4	4/4
3	1/2 ^a	0/2 ^a	2/4
6	0/3 ^b	0/3 ^b	3/4
9	3/3	0/3	3/3
12	3/3	0/3	3/3

500 ^aTwo or ^bone rabbits are dead before the third week
of CCl₄ injection.

501 **Table 2:** Grade of fibrosis in the liver according to the Ishak grading.

502

Weeks of CCl4 injection	0	3	6	9	12
Number of rabbits	4	2	3	3	3
Grade 0 (control)	4	-	-	-	-
Grade 1	-	2	-	-	-
Grade 2	-	-	2	-	-
Grade 3	-	-	1	1	-
Grade 4	-	-	-	1	2
Grade 5	-	-	-	1	1
Grade 6 (cirrhosis)	-	-	-	-	-

503

504 **Table 3:** Mean and standard deviation of QUS parameters (Young's mod-
505 ulus, ESD and EAC) estimated for different fibrosis grades and their
506 statistical significance.

507

Fibrosis grade	Young's modulus (kPa)	QUS parameters 10-20 MHz		QUS parameters 10-40 MHz	
		ESD (μm)	EAC (dB/cm ³)	ESD (μm)	EAC (dB/cm ³)
		Grade 0	5.89 \pm 1.34	22.6 \pm 1.9	49.0 \pm 2.3
Grade 1	7.93 \pm 1.62	34.9 \pm 2.4	45.9 \pm 1.5	26.7 \pm 0.7	50.6 \pm 1.0
Grade 2	9.25 \pm 1.76	31.8 \pm 2.4	45.7 \pm 1.8	25.0 \pm 1.2	50.4 \pm 0.5
Grade 3	10.07 \pm 1.83	31.0 \pm 1.6	44.7 \pm 0.8	26.1 \pm 0.9	47.5 \pm 0.9
Grade 4	11.46 \pm 1.94	33.6 \pm 3.0	44.6 \pm 1.1	26.1 \pm 2.0	48.9 \pm 1.0
Grade 5	12.99 \pm 2.07	33.4 \pm 3.1	43.9 \pm 1.3	25.9 \pm 1.3	48.3 \pm 0.7
<i>p</i> -values					
G0 vs G1	0.0026	0.0001	0.0320	0.0001	0.0135
G0 vs [G1-2]	0.0000	0.0000	0.0068	0.0000	0.0001
G0 vs [G3-5]	0.0000	0.0000	0.0000	0.0000	0.0000
[G1-2] vs [G3-5]	0.0000	0.5926	0.0484	0.9559	0.0000
G2 vs G3	0.3939	0.6991	0.3939	0.0931	0.0022

508 **Figure Captions**

509 **Figure 1:** *In vivo* and *ex vivo* observations of healthy and fibrotic livers.

510 Representative anatomical ultrasound images of healthy (a) and fibrotic
511 (grade 5) liver (b). Representative macroscopic images of healthy (c)
512 and fibrotic (grade 5) liver (d).

513 **Figure 2:** Examples of histological images of healthy and fibrotic livers
514 stained using hematoxylin/eosin and picrosirius red.

515 **Figure 3:** Representative shear wave elastography images of *ex vivo* healthy
516 and fibrotic livers.

517 **Figure 4:** Typical examples of measured BSCs from *ex vivo* healthy and
518 fibrotic livers using the two probes of center frequencies 20-MHz and
519 40-MHz. Also represented are the fitted curves with the SGM (dotted
520 line) and with the polydisperse Structure Factor Model SFM (dashed
521 line) for the healthy liver. The SGM estimates the ESD and EAC,
522 whereas the polydisperse SFM estimates the scatterer size distribution,
523 the volume fraction ϕ and the relative impedance difference γ_z .

524 **Figure 5:** Representative B-mode images obtained from *ex vivo* healthy and
525 fibrotic livers using the probe of center frequency 40-MHz.

526 **Figure 6:** (a) and (b) Confusion matrices obtained from the separation in
527 training and validation groups when considering the Young's modulus
528 E alone and the spectral-QUS parameters alone. (c), (d) and (e) Con-
529 fusion matrices obtained from the leave-one-out cross-validation when
530 considering the Young's modulus E alone, the spectral-QUS parameters

531 alone and the combination of spectral-QUS parameters with Young's
532 modulus. Also given are the percentages of correctly classified lobes,
533 denoted P_c .

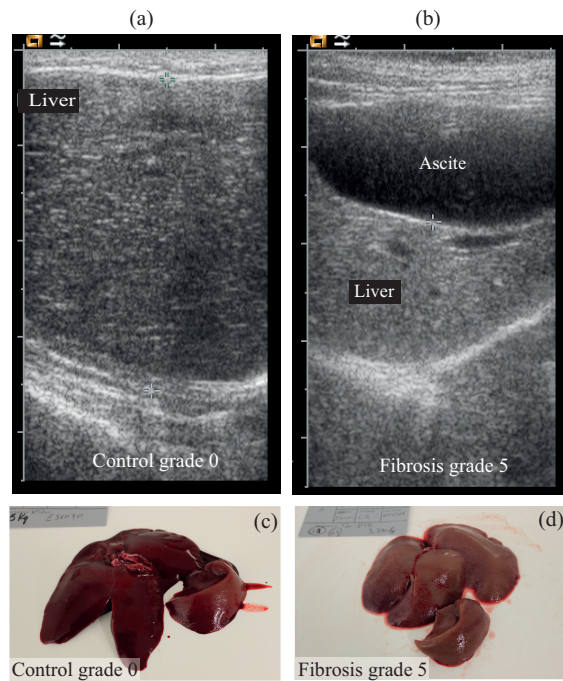


Figure 1: *In vivo* and *ex vivo* observations of healthy and fibrotic (grade 5) livers. Representative anatomical ultrasound images of healthy (a) and fibrotic liver (b). Representative macroscopic images of healthy (c) and fibrotic liver (d).

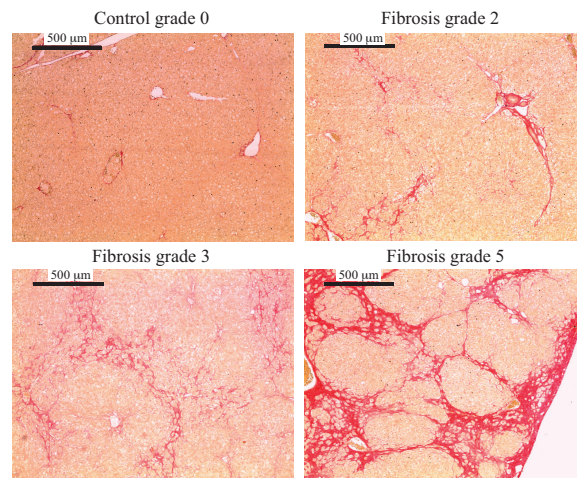


Figure 2: Examples of histological images of healthy and fibrotic livers stained using hematoxylin/eosin and picosirius red.

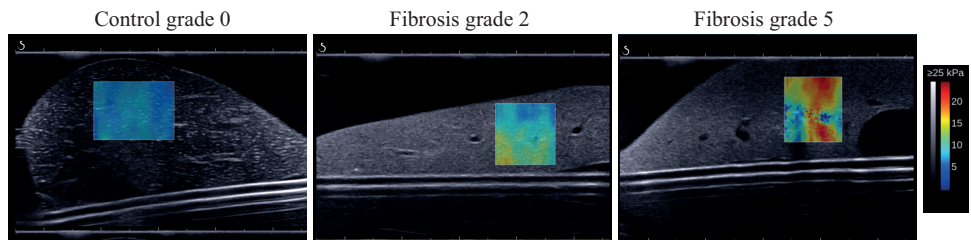


Figure 3: Representative shear wave elastography images of *ex vivo* healthy and fibrotic livers.

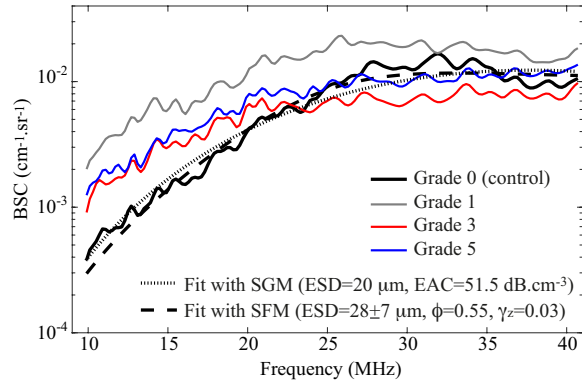


Figure 4: Typical examples of measured BSCs from *ex vivo* healthy and fibrotic livers using the two probes of center frequencies 20-MHz and 40-MHz. Also represented are the fitted curves with the SGM (dotted line) and with the polydisperse Structure Factor Model SFM (dashed line) for the healthy liver. The SGM estimates the ESD and EAC, whereas the polydisperse SFM estimates the scatterer size distribution, the volume fraction ϕ and the relative impedance difference γ_z .

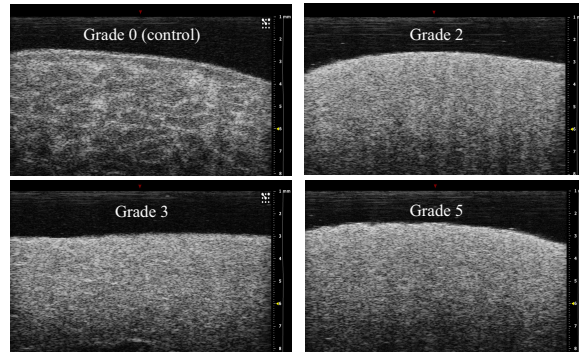


Figure 5: Representative B-mode images obtained from *ex vivo* healthy and fibrotic livers using the probe of center frequency 40-MHz.

a) Young's modulus E					
		Assigned			P_c
		G0	G1-2	G3-5	
Actual	G0	14	4	0	77.8%
	G1-2	0	15	3	83.3%
	G3-5	0	4	27	87.1%

b) ESD and EAC (10-20 MHz)					
		Assigned			P_c
		G0	G1-2	G3-5	
Actual	G0	18	0	0	100%
	G1-2	0	12	6	66.7%
	G3-5	0	7	24	77.4%

c) Young's modulus E					
		Assigned			P_c
		G0	G1-2	G3-5	
Actual	G0	8	4	0	66.7%
	G1-2	0	11	1	91.7%
	G3-5	0	7	14	66.7%

d) ESD and EAC (10-20 MHz)					
		Assigned			P_c
		G0	G1-2	G3-5	
Actual	G0	10	0	2	83.3%
	G1-2	0	7	5	58.3%
	G3-5	0	8	13	61.9%

e) Young's modulus E , ESD and EAC (10-20 MHz)					
		Assigned			P_c
		G0	G1-2	G3-5	
Actual	G0	12	0	0	100%
	G1-2	0	11	1	91.7%
	G3-5	0	7	14	66.7%

Figure 6: (a) and (b) Confusion matrices obtained from the separation in training and validation groups when considering the Young's modulus E alone and the spectral-QUS parameters alone. (c), (d) and (e) Confusion matrices obtained from the leave-one-out cross-validation when considering the Young's modulus E alone, the spectral-QUS parameters alone and the combination of spectral-QUS parameters with Young's modulus. Also given are the percentages of correctly classified lobes, denoted P_c .